

Supplementary Information

Synthesis of Photo-responsive and Photoluminescent In_2S_3 ultrathin nanosheets achieved through a new single source molecular precursor

Gourab Karmakar,^{a,b} Adish Tyagi,^{*a,b} Alpa Y. Shah,^a Liladhar B. Kumbhare,^a A. P. Wadawale,^a G. Kedarnath,^{*a,b} Vishal Singh^c

^a*Chemistry Division, Bhabha Atomic Research Centre, Mumbai- 400 085 (India),*

^b*Homi Bhabha National Institute, Anushaktinagar, Mumbai- 400 094 (India)*

^c*Materials Science Division, Bhabha Atomic Research Centre, Mumbai- 400 085 (India).*

Email: tyagia@barc.gov.in, kedar@barc.gov.in

Determination of band gap from Brus equation

The Brus equation is given by¹

$$E_{np} \approx E_g(0) + \frac{\hbar^2 \pi^2}{2r^2} \left(\frac{1}{m_e^*} + \frac{1}{m_h^*} \right) - \frac{1.8e^2}{4\pi\epsilon R}$$

where E_{np} is the bandgap of the NSs, E_g is the band gap of bulk In_2S_3 (2.2 eV), $\hbar = h/2\pi$ is the reduced Planck constant, e is the electron charge, m_e^* is the effective mass of electron, m_h^* is the effective mass of hole, $m_e^* = m_h^*$ (0.25×10^{-28} g), r is the average crystallite size of the NSs and ϵ is the dielectric constant ($\epsilon = 11$). Putting all the values, the direct band gap of the ultrathin In_2S_3 NSs comes out to be ~2.51 eV.

Calculation of exciton Bohr radius of In_2S_3

The Bohr radius of the exciton in In_2S_3 can be calculated by the following equation²

$$r_B = \frac{\hbar^2 \epsilon}{e^2} \left(\frac{1}{m_e} + \frac{1}{m_h} \right)$$

where ϵ is the dielectric constant (~11), \hbar is the Planck constant and m_e and m_h are the electron and hole effective mass, respectively. $m_e = m_h = \mu = 0.25 \times 10^{-28}$ g. From these data, Bohr radius of the exciton in In_2S_3 is calculated to be 33.6 nm.

Figure Captions:

Fig. S1. Molecular structure of $\text{In}[\text{Me}_2\text{NCH}(\text{Me})\text{CH}_2\text{S}]_2\text{Cl}$ (**1**) showing envelop conformation of the ligands.

Fig. S2. Thermogravimetric analysis of $\text{In}[\text{Me}_2\text{NCH}(\text{Me})\text{CH}_2\text{S}]_2\text{Cl}$ (**1**)

Fig. S3. EDS analysis of In_2S_3 NSs synthesized from $\text{In}[\text{Me}_2\text{NCH}(\text{Me})\text{CH}_2\text{S}]_2\text{Cl}$ (**1**) at 150°C for 1 minute.

Fig. S4. XPS survey scan of In_2S_3 NSs synthesized from $\text{In}[\text{Me}_2\text{NCH}(\text{Me})\text{CH}_2\text{S}]_2\text{Cl}$ (**1**) at 150°C for 1 minute.

Fig. S5. 2D elemental mapping of In_2S_3 NSs synthesized from $\text{In}[\text{Me}_2\text{NCH}(\text{Me})\text{CH}_2\text{S}]_2\text{Cl}$ (**1**) at 150°C for 1 minute.

Fig. S6. I-V characteristics of the In_2S_3 NSs synthesized from $\text{In}[\text{Me}_2\text{NCH}(\text{Me})\text{CH}_2\text{S}]_2\text{Cl}$ (**1**) at 150°C for 1 minute.

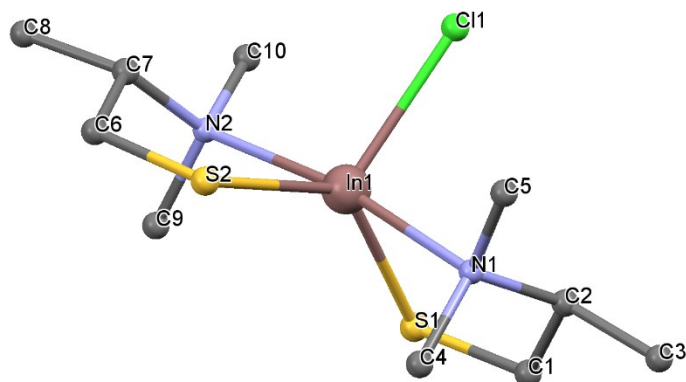


Fig. S1. Molecular structure of $\text{In}[\text{Me}_2\text{NCH}(\text{Me})\text{CH}_2\text{S}]_2\text{Cl}$ (**1**) showing envelop conformation of the ligands.

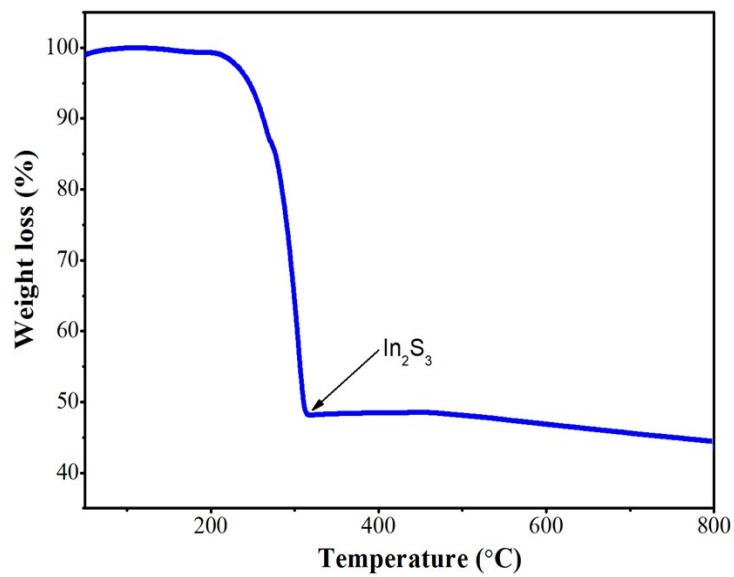


Fig. S2. Thermogravimetric analysis of $\text{In}[\text{Me}_2\text{NCH}(\text{Me})\text{CH}_2\text{S}]_2\text{Cl}$ (**1**)

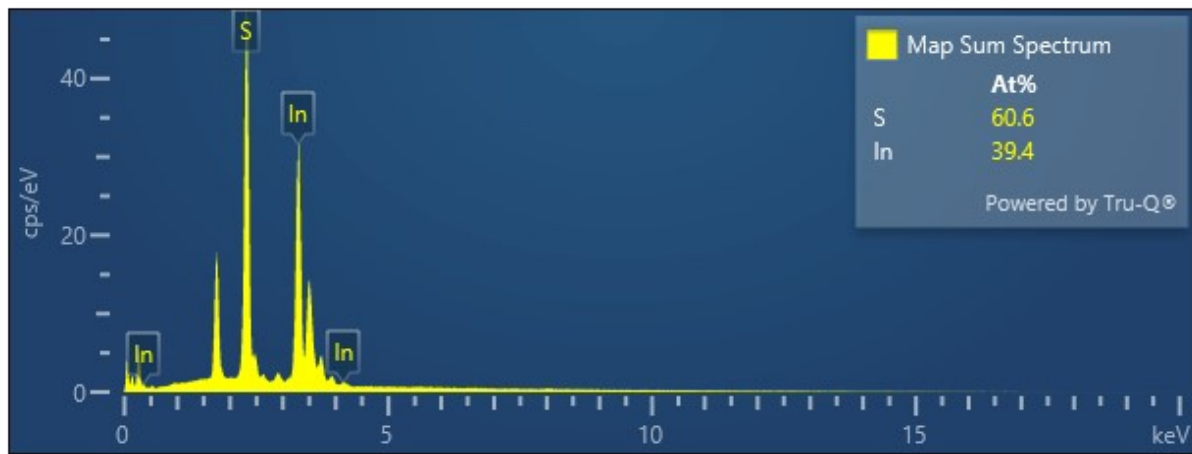


Fig. S3. EDS analysis of In_2S_3 NSs synthesized from $\text{In}[\text{Me}_2\text{NCH}(\text{Me})\text{CH}_2\text{S}]_2\text{Cl}$ (**1**) at 150°C for 1 minute.

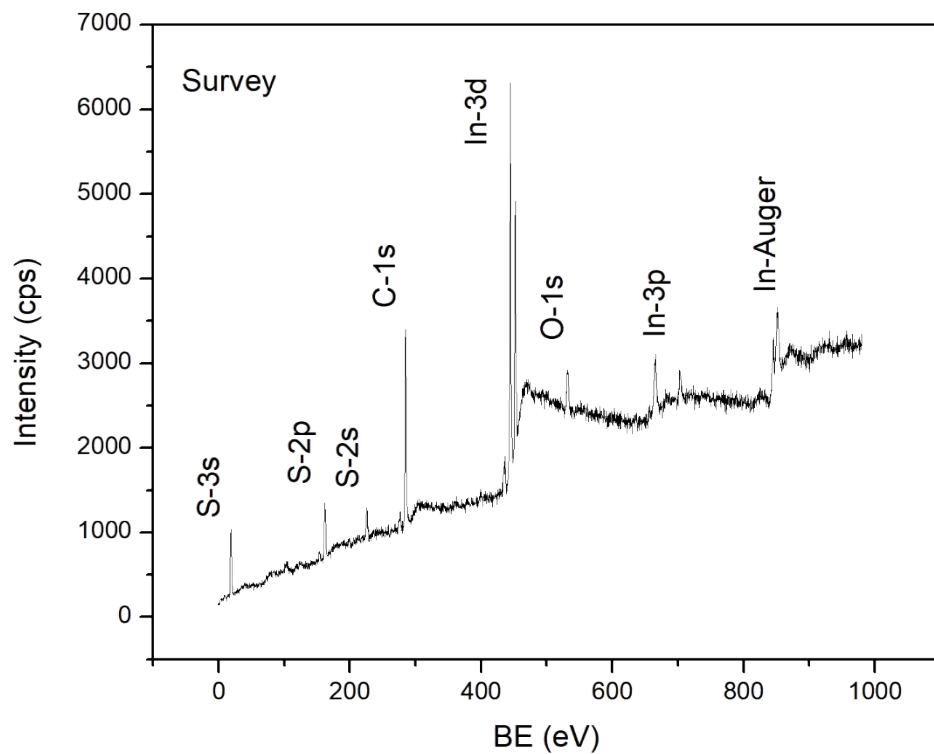


Fig. S4. XPS survey scan of In_2S_3 NSs synthesized from $\text{In}[\text{Me}_2\text{NCH}(\text{Me})\text{CH}_2\text{S}]_2\text{Cl}$ (**1**) at 150°C for 1 minute.

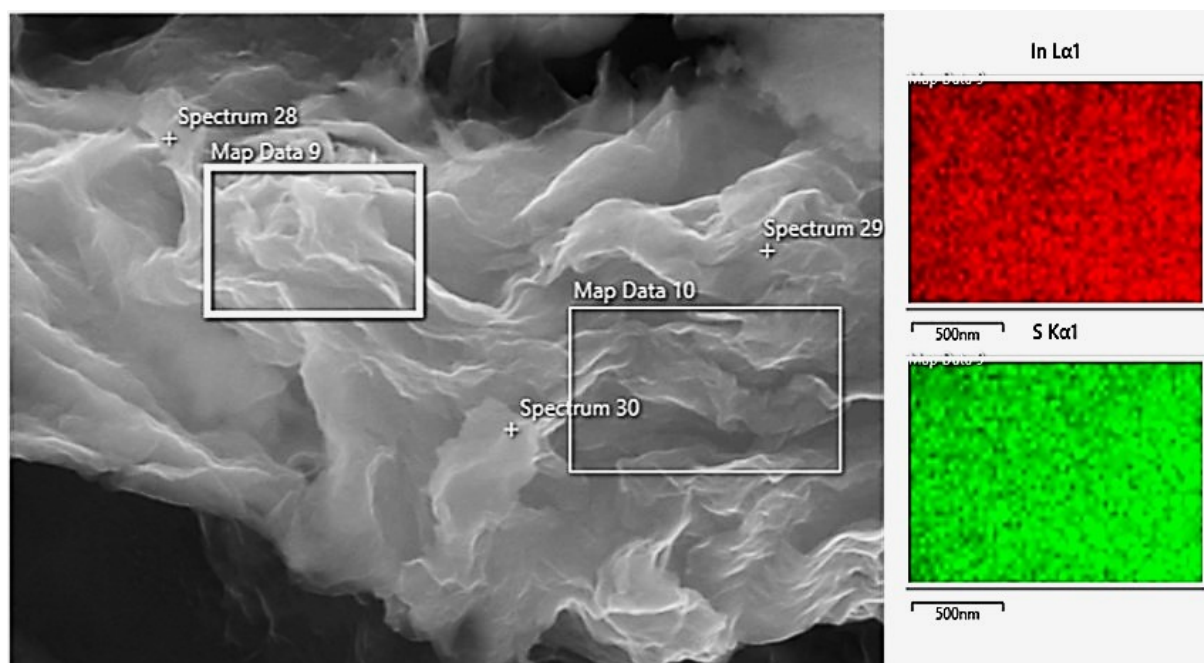


Fig. S5. 2D elemental mapping of In_2S_3 NSs synthesized from $\text{In}[\text{Me}_2\text{NCH}(\text{Me})\text{CH}_2\text{S}]_2\text{Cl}$ (**1**) at 150°C for 1 minute.

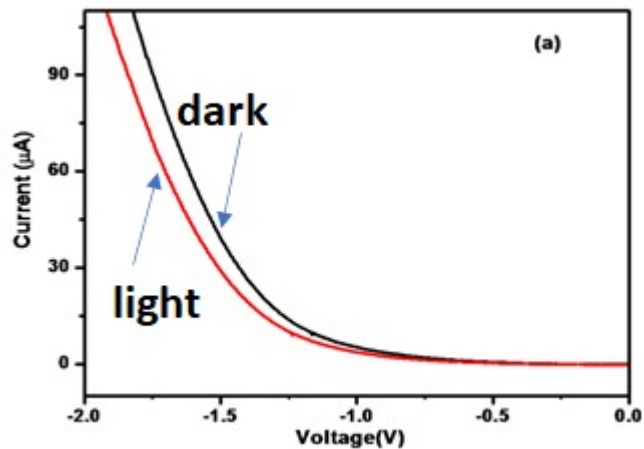


Fig. S6. I-V characteristics of the In_2S_3 NSs synthesized from $\text{In}[\text{Me}_2\text{NCH}(\text{Me})\text{CH}_2\text{S}]_2\text{Cl}$ (**1**) at 150°C for 1 minute.

References:

1. R. Li, L. Tang, Q. Zhao, T. H. Ly, K. S. Teng, Y. Li, Y. Hu, C. Shu and S. P. Lau, *Nanoscale Res. Lett.*, 2019, **14**, 161.
2. W. Chen, J.-O. Bovin, A. G. Joly, S. Wang, F. Su and G. Li, *J. Phys. Chem. B*, 2004, **108**, 11927-11934.